# Electrostatic Interaction of Colloidal Surfaces with Variable Charge

**Sven Holger Behrens* and Michal Borkovec†**

*Department of Chemistry, Clarkson University, Potsdam, New York 13699-5814, and Swiss Federal Institute of Technology, ETHZ-ITO, Grabenstrasse 3, 8952 Schlieren, Switzerland*

*Received: October 21, 1998*

When two surfaces with ionizable groups interact across an electrolyte solution, both their equilibrium charge density and the corresponding electrostatic surface potential will depend on the surface separation (charge regulation). The corresponding nonlinear boundary conditions are often replaced, for simplicity, by the limiting conditions of constant charge or constant surface potential. A strategy to linearize the boundary conditions, initially devised for the case of low potentials only, has recently been adapted to situations of arbitrary potential. Within a 1-p*K* Basic Stern Model suitable for a large class of surface materials, we now address the implications of charge regulation on the level of Poisson−Boltzmann theory. The regulation behavior can be characterized in terms of a single parameter taking values between 0 for constant potential and 1 for constant charge conditions. This parameter depends on the capacities associated with the diffuse part and the compact part of the electrical double layer and can be inferred from acid−base titrations. We discuss the effect of regulation on a variety of measurable quantities for exemplary surfaces of carboxyl latex, silica, and iron hydroxide.

## 1. Introduction

The interaction between electrically charged surfaces across a liquid is of central interest to colloid science and electrochemistry; it is also relevant to biophysics, environmental science, and materials engineering. A common modeling strategy starts by splitting the net pair interaction into a purely electrostatic double layer contribution, a term due to dispersion forces, and possibly further contributions, that are all tackled separately.[1,2] This separation is a delicate issue and by no means undisputed,[3] but it has enormously promoted our understanding of colloidal and polymeric systems, and shall be adopted for the following discussion as well.

In the classical theory proposed by Derjaguin, Landau, Verwey, and Overbeek (DLVO), the double-layer term is calculated on a mean field level from the solution of the Poisson−Boltzmann equation for the electrostatic potential.[4,5] A common and computationally convenient choice of boundary conditions fixes either the electrostatic surface potential or the surface charge density, irrespective of the surface separation. For most surfaces, however, the very nature of the material suggests a more complex relation between the charge density and the surface potential,[6] both properties being adjusted simultaneously as the surfaces approach each other. This effect directly influences a wealth of measurable quantities that characterize colloidal systems, such as the swelling pressure in lamellar phases, the force, and interaction energy between charged surfaces or the rates of aggregation of colloidal particles.

Many previous studies have considered surfaces with ionizable groups maintaining chemical equilibrium at all surface separations, in general referred to as charge-regulating surfaces.[6−16] The corresponding nonlinear boundary conditions complicate the calculation of interaction energies, but the two simpler scenarios of constant charge (cc) and constant potential (cp) are known to provide an upper and a lower limit for the electrostatic repulsion of identically charged surfaces.[9] Hence the question arises, whether for a given system these two limiting cases lead to very different predictions for the measurable properties of interest and, if so, where between the two limiting cases the system actually lies.

The Debye−Hückel approximation with a general linearized boundary condition, has exhaustively been discussed by Carnie and Chan.[12] We have recently extended this approach for arbitrary surface potentials and shown that, as in the framework of Debye−Hückel theory, the regulation behavior is determined by the competition of the diffuse layer capacity $C^{D}$ and the capacity $C^{I}$ of the inner (compact) layer.[17]

The inner layer capacity is closely related to the slope of the familiar charging curves obtained in acid−base titrations. We can therefore predict the dependence of surface properties and interaction on the surface separation, once we know how the charge of the *isolated* surface varies with pH. For $C^{I} \gg C^{D}$ the constant potential behavior will be found; in the opposite case, $C^{I} \ll C^{D}$, two surfaces will interact at constant charge. The implications for a variety of measurable quantities shall be discussed in the exemplary cases of an iron hydroxide, a carboxyl latex and a silica surface, using the exact solution to the Poisson−Boltzmann equation under conditions of charge regulation.

## 2. Fundamentals

Consider two equally charged, parallel plane surfaces immersed in an electrolyte solution. The liquid in the gap between the surfaces shall be in equilibrium with a solution reservoir. Surface charge will give rise to an electric double layer that consists of an inner (compact) part, characterized by the chemical properties of the surface material, and a diffuse part built up of the mobile ions in the solution. We may think of these two parts, the compact and the diffuse layer, as of two adjacent subsystems, each of which is described by its own equation of state. Equilibrium between the two layers then

* To whom correspondence should be addressed. E-mail: behrens@ito.umnw.ethz.ch.

† Dept. of Chemistry, Clarkson University, Potsdam, New York 13699-5814.

10.1021/jp984099w CCC: $18.00 
Published on Web 03/03/1999

requires that the equations of state be respected *simultaneously* for both subsystems.

**2.1. Inner (Compact) Layer.** Let the state of the surface depend on just one type of basic or acidic surface headgroup undergoing a one step protonation or deprotonation reaction

$$\mathrm{AH} \rightleftharpoons \mathrm{A} + \mathrm{H} \tag{1}$$

where AH and A are the protonated and deprotonated form of the surface groups. (The description is not necessarily restricted to the case of protons as the potential determining ions.) This simple picture is realistic at best, if only monovalent ions are present. In the presence of polyvalent ions, the description is complicated by competitive adsorption processes and a possible breakdown of the Poisson−Boltzmann treatment due to ion−ion correlations. Following a common strategy,[8] we shall further neglect the discrete nature of the surface sites and assume the charges to be uniformly smeared out. The charging state of the surface is then determined exclusively by the average proton density at the surface, which we will denote by $\Gamma_{AH}$. This property is related to the charge density $\sigma$ via

$$\sigma = e(\Gamma_{AH} - \Gamma_{ref}) \tag{2}$$

where $e$ is the protonic charge and $\Gamma_{ref}$ the proton density of the uncharged surface. The deprotonation reaction will be described by a mass action law

$$\frac{(\Gamma_{tot} - \Gamma_{AH})\, a_H^{(0)}}{\Gamma_{AH}} = K \tag{3}$$

where $a_H^{(0)}$ has been introduced as the "proton activity at the surface" by Healy and White,[8] $\Gamma_{tot}$ is the total site density and $K$ the dissociation constant. To derive the charge−potential relation, we have to specify a model for the inner layer.

*Gouy−Chapman Model.* The simplest description compatible with our previous assumptions places all the surface charge into one plane (characterized by the electrostatic potential $\psi_0$). The surface proton activity in eq 3 is related to the bulk activity $a_H$ via

$$a_H^{(0)} = a_H \exp(-\beta e \psi_0) \tag{4}$$

$\beta^{-1} = k_B T$ being the thermal energy. In this model, the diffuse layer with the electrostatic potential $\psi_d$ at its head end extends all the way to the plane of charge, so we have

$$\psi_d = \psi_0 \tag{5}$$

This simple picture for the surface region has been called Gouy−Chapman model[8,18] or diffuse layer model,[19] because this model is used together with the Gouy−Chapman theory for the diffuse layer near a single charged plane.[20] Combining eqs 2 through 5 yields

$$\sigma = \frac{e\Gamma_{tot}}{1 + \exp[\beta e(\psi_d - \psi_N)]} - e\Gamma_{ref} = \sigma^I(\psi_d) \tag{6}$$

where

$$\psi_N = (\mathrm{pK} - \mathrm{pH})\frac{\ln 10}{\beta e} \tag{7}$$

is just the Nernst potential, and we have labeled the functional dependence of $\sigma$ on $\psi_d$ (for later distinction) by the superscript I because it is determined by the *inner* part of the electric double layer. (We have used the common notation $\mathrm{pH} = -\log_{10} a_H$ and $\mathrm{pK} = -\log_{10} K$.) As will become apparent later, eq 6 describes the so-called "mastercurve" of the charging functions observed in acid−base titrations.[21,22]

*Basic Stern Model.* A useful generalization of the Gouy−Chapman approach is achieved in the so-called basic Stern Model,[19] also referred to as zeroth-order Stern model.[8] In this model, all *nonadsorbed* ions are pictured to have at least some finite minimum distance from the plane of charge, corresponding to the ionic radius. The diffuse part of the electric double layer is separated from this plane by a charge-free Stern layer, which acts like a parallel plate capacitor between the mobile and the bound charge. Accordingly, the electrostatic potential is assumed to drop linearly from its plane of charge value $\psi_0$ to its value $\psi_d$ at the onset of the diffuse layer, and the ratio of the charge to this potential drop defines the Stern capacity[23]

$$\sigma = C^S(\psi_0 - \psi_d) \tag{8}$$

For simplicity and in a first approximation, we shall subsequently account for the presence of a Stern layer through eq 8 only, but neglect the actual thickness of that layer. With eq 8 instead of eq 5, the relation between $\sigma$ and $\psi_d$ (eq 6) is given by

$$\psi_d = \psi_N - \frac{\sigma}{C^S} + \frac{1}{\beta e}\ln\frac{e(\Gamma_{tot} - \Gamma_{ref}) - \sigma}{e\Gamma_{ref} + \sigma} \tag{9}$$

This relation now defines the function $\sigma^I(\psi_d)$ for the basic Stern model. In the limit of an infinite Stern capacity, we recover the Gouy−Chapman model. Another limiting case can be realized for small Stern capacity: When the third term on the right-hand side of eq 9 is very small compared to the second term, then the Nernstian surface,

$$\sigma = C^S(\psi_N - \psi_d) \tag{10}$$

will be a good approximation. It is well-known that amphoteric systems can be described that way; we immediately understand this from eq 9 because for those systems $\Gamma_{tot} \simeq 2\Gamma_{ref}$ and typically $\sigma \ll e\Gamma_{tot}/2$ for a wide range of pH around the point of zero charge. However, for surfaces that are uncharged when fully protonated or fully deprotonated ($\Gamma_{ref} = \Gamma_{tot}$ or $\Gamma_{ref} = 0$), the Nernst approximation will fail.

**2.2. Diffuse Layer.** A different charge−potential relation is imposed by the *diffuse* part of the double layer. The distribution of mobile ions is governed, as we have assumed, by the Poisson−Boltzmann equation

$$\frac{d^2\psi}{dx^2} = \frac{\kappa^2}{\beta e}\sinh(\beta e\psi) \tag{11}$$

where $\psi(x)$ is the electrostatic potential as a function of the distance $x$ normal to the surface and $\kappa^{-1}$ is the Debye length defined by $\kappa^2 = 2\beta e^2 n/(\epsilon\epsilon_0)$ ($n$ being the bulk electrolyte concentration and $\epsilon\epsilon_0$ the permittivity of the solution). When the midplane is chosen as origin, then the symmetry of the problem implies that $\psi(x) = \psi(-x)$ and the surfaces will be located at $x = \pm L/2$ where the potential is just the diffuse layer potential $\psi_d = \psi(L/2)$. The surface charge density is given by $\sigma = \epsilon\epsilon_0 d\psi/dx$ at $x = L/2$.

*Debye−Hückel Limit.* We shall first discuss the linearized form of eq 11. When the electrostatic potential is small, the

Poisson−Boltzmann equation is approximated well by the Debye−Hückel equation (DH)

$$\frac{d^2\psi}{dx^2} = \kappa^2\psi \tag{12}$$

Straightforward integration yields

$$\psi(x) = \psi_d \frac{\cosh(\kappa x)}{\cosh(\kappa L/2)} \tag{13}$$

from which the charge density follows as

$$\sigma = \epsilon\epsilon_0\kappa\psi_d \tanh(\kappa L/2) \tag{14}$$

This relation between $\sigma$ and $\psi_d$ has been named $\sigma^D(\psi_d,L)$ to stress that it originates from the *diffuse* part of the double layer.

*Poisson−Boltzmann Description.* Just as in the Debye−Hückel limit, the differential eq 11 engenders a relation of the form

$$\sigma = \sigma^D(\psi_d,L) \tag{15}$$

In the limit of large surface separations, this relation is reduced to the familiar result for an isolated surface, called the Grahame equation[1]

$$\sigma^D(\psi_d,\infty) = \lim_{L\to\infty}\sigma^D(\psi_d,L) = \frac{2\epsilon\epsilon_0\kappa}{\beta e}\sinh(\beta e\psi_d/2) \tag{16}$$

The corresponding relation for interacting surfaces was obtained by Ninham and Parseggian,[6] a derivation of the expressions cited below is outlined in the Appendix. For a finite separation $L$, the electric potential at point $x$ between the surfaces is given by

$$\psi(x) = \psi_m + \frac{2}{\beta e}\ln \mathrm{cd}(u|m) \tag{17}$$

where $\psi_m$ is the midplane potential $\psi_m = \psi(0)$, and $\mathrm{cd}(u|m)$ is a Jacobian elliptic function of argument $u$ and parameter $m$ (in standard notation, see Appendix) with $u = \kappa x/[2\exp(\beta e\psi_m/2)]$ and $m = \exp(2\beta e\psi_m)$. Equation 17 corresponds to eq 13 in the Debye−Hückel case. It follows that the charge density is related to the diffuse layer potential $\psi_d$ by the following two equations[6]

$$\sigma = \frac{\epsilon\epsilon_0\kappa}{\beta e}\frac{\exp(2\beta e\psi_m) - 1}{\exp(\beta e\psi_m/2)}\frac{\mathrm{sn}(v|m)}{\mathrm{cn}(v|m)\,\mathrm{dn}(v|m)} \tag{18}$$

and

$$\psi_d = \psi_m + \frac{2}{\beta e}\ln \mathrm{cd}(v|m) \tag{19}$$

where $\mathrm{sn}(v|m)$, $\mathrm{cn}(v|m)$, $\mathrm{dn}(v|m)$, and $\mathrm{cd}(v|m)$ are Jacobian elliptic functions of argument $v$ and parameter $m$ (see Appendix); now they must be taken at $v = \kappa L/[4\exp(\beta e\psi_m/2)]$. Together, eqs 18 and 19 define our relation $\sigma = \sigma^D(\psi_d,L)$ in analogy to eq 14. The above expressions, although not analytical, are straightforward to implement, the Jacobian elliptic functions being standard functions[24] that are generated by modern mathematical libraries.

**2.3. Equilibrium Point.** Both charge−potential relations $\sigma^I(\psi_d)$ and $\sigma^D(\psi_d,L)$ are represented schematically in Figure 1. The function $\sigma^I(\psi_d)$ always decreases monotonically with increasing $\psi_d$; it is shown (a) for the case of a surface that is uncharged when fully deprotonated ($\Gamma_{ref} = 0$ in eq 9) and (b) for an amphoteric surface with $\Gamma_{ref} = \Gamma_{tot}/2$. The graph of $\sigma^D(\psi_d,L)$ is shown both for infinite surface separation and for a finite separation $L$. The dotted straight lines correspond to the Debye−Hückel version of these two curves (eq 14). Equating the charge of the compact and the diffuse layer means to apply the boundary condition 9 to eq 11. The second boundary condition originates from the spatial symmetry of the system. The equilibrium point

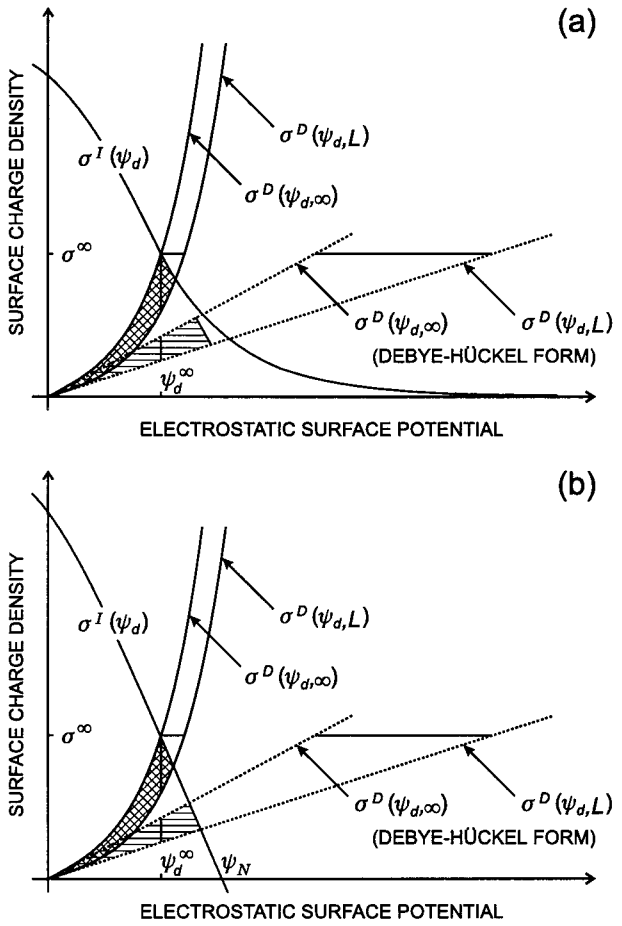


**Figure 1.** Schematic representation of the charge-potential relations $\sigma^I(\psi_d)$ and $\sigma^D(\psi_d,L)$ for the case (a) where surfaces are uncharged when fully deprotonated ($\Gamma_{ref} = 0$), and (b) for an amphoteric surface. In both cases the intersection of $\sigma^I(\psi_d)$ and $\sigma^D(\psi_d,L)$ corresponds to the equilibrium value of the surface charge and potential, the (cross-)hatched area between the curves is a measure of the interaction energy. The curve $\sigma^I(\psi_d)$ is replaced by the vertical line at $\psi_d = \psi_d^\infty$ in the constant potential limit and by the horizontal line through $\sigma = \sigma^\infty$ in the constant charge limit; for the regulated case, $\sigma^I(\psi_d)$ is approximated by its tangent in the equilibrium point for infinite separation.

$$\sigma^I(\psi_d) \equiv \sigma^D(\psi_d,L)\ \text{(equilibrium)} \tag{20}$$

is apparent in Figure 1 as the intersection of the curves $\sigma^D(\psi_d,L)$ and $\sigma^I(\psi_d)$. In the case of constant charge conditions, the function $\sigma^I(\psi_d)$ is replaced by the function $\sigma^I(\psi_d) = \sigma^\infty =$ constant; in the constant potential case, $\sigma^I(\psi_d)$ is replaced by the vertical line $\psi_d = \psi_d^\infty = \text{const}$.

It can be shown that, as the surface separation decreases, $\sigma^D(\psi_d,L)$ also decreases and tends to zero for all $\psi_d$ in the limit of contacting surfaces (see Appendix); thus,

$$\sigma \to 0 \qquad \text{as } L \to 0 \tag{21}$$

This relation can be understood from Figure 1, since when the

surfaces are getting closer, the equilibrium point moves along the curve $\sigma^I(\psi_d)$ toward the $\psi_d$-axis where $\sigma = 0$. If $\sigma^I(\psi_d)$ reaches the axis only asymptotically, as in Figure 1a, then the surface potential will diverge upon contact. If, on the other hand, $\sigma^I(\psi_d)$ goes through zero at a finite value of $\psi_d$, then this value of the potential will be assumed by the surfaces in contact; such is the case for an amphoteric surface ($\Gamma_{ref} = \Gamma_{tot}/2$) where $\psi_d \rightarrow \psi_N$ as $L \rightarrow 0$ (Figure 1c).

**2.4. Forces and Energies.** In order to see how the interaction of the surfaces is affected by the charge regulation, we have to calculate the interaction free energy $W(L)$ (per unit area) as a function of the separation $L$. One way of doing so, is to integrate the difference in pressure due to the charged surfaces over the surface distance

$$W(L) = \int_L^\infty \Pi(L')\, dL' \tag{22}$$

In our notation, the pressure difference simply reads[6]

$$\Pi(L) = 2nk_BT\,[\cosh(\beta e\psi_m(L)) - 1] \tag{23}$$

where $n$ is the number density of cations in the bulk.[1]

Within the Derjaguin approximation, the energy $W(L)$ given by eq 22 is proportional to the force $F$ between two crossed cylinders or a sphere and a plane of the same surface charge $\sigma$; in either case

$$F(L)/R = 2\pi W(L) \tag{24}$$

where $R$ is the radius of the sphere (or the cylinders). The calculated energy $W(L)$ therefore lends itself to comparison with experimental forces observed with the surface force apparatus or the atomic force microscope.[25,26] A similar argument applies to the case of two spheres of radii $R_1$ and $R_2$ and leads to the sphere−sphere interaction potential

$$V(L) = 2\pi \frac{R_1R_2}{R_1 + R_2} \int_L^\infty W(L')\, dL' \tag{25}$$

This pair interaction energy $V(L)$ is accessible to measurements with optical tweezers[27] or total internal reflection microscopy.[28] It is also an essential input in the calculation of aggregation rates for colloidal suspensions.[29]

## 3. Regulation Criterion

An equivalent way to compute the double layer interaction uses the charging integral.[5] Chan and Mitchell[9] have taken this approach to show that, for identical surfaces, the interaction energy $W(L)$ per unit area (eq 22) can be represented graphically as twice the area between the curves $\sigma^D(\psi_d,L)$, $\sigma^D(\psi_d,\infty)$, and $\sigma^I(\psi_d)$, i.e., the crosshatched area of Figure 1. The area we obtain if $\sigma^I(\psi_d)$ is replaced by the curves $\psi_d = \psi_d^{(cp)}$ = constant or $\sigma = \sigma^{(cc)}$ = constant (a vertical or horizontal line in Figure 1) corresponds to (half of) the constant potential or constant charge value of $W$, and obviously,

$$W^{(cp)}(L) \le W^{(reg)}(L) \le W^{(cc)}(L)$$

The fraction of $W^{(cc)} - W^{(cp)}$ which actually contributes to the interaction energy of the regulating surfaces is given by the function

$$p(L) = \frac{W^{(reg)}(L) - W^{(cp)}(L)}{W^{(cc)}(L) - W^{(cp)}(L)} \tag{26}$$

taking values between 0 for constant potential and 1 for constant charge conditions.

For sufficiently large separations, this fraction $p(L)$ mainly depends on the local shape of the functions $\sigma^I(\psi_d)$ and $\sigma^D(\psi_d,L)$ around the equilibrium point for isolated surfaces. We have proposed a local linearization of both charge−potential relationships, allowing for arbitrary values of the equilibrium surface potential.[17] Geometrical arguments indicate that, for an interesting range of separations $L$, the fraction $p(L)$ (eq 26) may be approximated by its large distance limit, the regulation parameter[17]

$$p = \lim_{L\rightarrow\infty} p(L) = \frac{C^D}{C^D + C^I} \tag{27}$$

where

$$C^D = \frac{\partial\sigma^D}{\partial\psi_d} = \epsilon\epsilon_0\kappa \cosh\left(\frac{1}{2}\beta e\psi_d^\infty\right) \tag{28}$$

is the diffuse layer capacity, and

$$C^I = -\frac{d\sigma^I}{d\psi_d} \tag{29}$$

is the capacity of the compact inner layer. In both expressions the derivative is evaluated at the equilibrium surface potential for $L \rightarrow \infty$. Thus, charge regulation is determined by the competition of two capacities that reflect how easily charge can be stored in either the compact or the diffuse layer. A comparatively large diffuse layer capacity ($p \approx 1$) leads to constant-charge-like behavior; when the capacity of the inner layer is dominant ($p \approx 0$), interaction will be constant-potential-like. Any intermediate behavior corresponds to a regulation parameter $p$ between 0 and 1.

This regulation criterion, eq 27, generalizes a result previously found by Carnie and Chan for the case of low potentials.[12] They showed that, on the level of Debye−Hückel theory and with a linearized relation $\sigma^I(\psi_d)$, the interaction energy per unit area (twice the horizontally hatched area between the dotted curves in Figure 1) is given by

$$W(L) = 2\epsilon\epsilon_0\kappa(\psi_d^\infty)^2\,[\exp(\kappa L) - 2p + 1]^{-1} \tag{30}$$

where, in linearizing $\sigma^D$ globally around $\psi_d = 0$, the hyperbolic cosine in eq 28 is dropped. In going to arbitrary potentials, we lose the ability of writing down the interaction energy explicitly; however, its location between the limits of constant charge or potential is still given by the same type of criterion.

## 4. Exemplary Systems

Some of the consequences of charge regulation shall be illustrated by looking at the concrete example of three different types of surface materials: carboxyl latex, silica, and an iron hydroxide. Typical parameters used to model these surfaces are summarized in Table 1.

**4.1. Three Generic Systems.** The first case we shall consider is carboxyl latex with the surface reaction

$$-\mathrm{COOH} \rightleftharpoons -\mathrm{COO}^- + \mathrm{H}^+ \tag{31}$$

and typically a relatively small density of surface groups. In account of experimental titration data that show carboxyl latex particles to be described well within the Gouy−Chapman model, we have chosen an infinite Stern capacity.[8,18,30]

**TABLE 1: Exemplary Materials**

| material | p$K$ | $\Gamma_{tot}$[a] ($nm^{-2}$) | ($\Gamma_{ref}/\Gamma_{tot}$)[b] | $C_S$[c] ($F/m^2$) | $A$[d] ($10^{-20}J$) |
|---|---|---|---|---|---|
| carboxyl latex | 4.9 | 0.574 | 1 | $\infty$ | 1.8 |
| silica | 7.5 | 8.00 | 1 | 2.9 | 0.83 |
| iron (hydr)oxide | 9.5 | 6.15 | 1/2 | 1.1 | 6.0 |

[a] Total density of surface headgroups. [b] Fraction of the total number of sites that are protonated in the zero charge configuration. [c] Stern capacity. [d] Hamaker constant across water.

The second example is a silica surface

$$Si-OH \rightleftharpoons Si-O^- + H^+ \tag{32}$$

which will be modeled with a finite Stern capacity and typically has a much higher density of chargeable sites than latex. These two types of surfaces are neutral at low pH and acquire a negative charge at high pH.[31] Our third example is an iron hydroxide surface

$$Fe-OH_2^{+1/2} \rightleftharpoons Fe-OH^{-1/2} + H^+ \tag{33}$$

where the partial charges result from the fractional valence of the Fe−O bonds.[32] This surface is positively charged at low pH and reverses its charge as the pH is increased. With the choice of $\Gamma_{tot}/2$ for the density of protonated sites in the uncharged state, the characteristics of this amphoteric surface can be rationalized in terms of the 1-p$K$ Basic Stern Model. The present model allows a rather good description of the charging behavior of goethite,[33] and with adjusted values for the p$K$ and the Stern capacity, it also works for gibbsite and rutile. (The simple 1-p$K$ model used here is essentially equivalent to the more common 2-p$K$ model.[34]) The most precarious aspect of our approach, when applied to metal hydroxides, is arguably the neglect of ion pair formation or specific adsorption of salt ions.[33] Also, the unaccounted presence of different crystal planes with different charging characteristics complicates the issue.[35] The incorporation of such effects into a theoretical treatment would go far beyond the scope of our present framework but likely not change the qualitative conclusions.

**4.2. Isolated Surfaces.** We use equations 9, 16, and 20 for all of our exemplary materials to determine the equilibrium charge density (in isolation) as a function of pH. The resulting titration curves at three ionic strengths are presented in Figure 2a (thin lines). They all agree well with experimental data.[30,31,33] If plotted as a function of the "surface pH " (or more precisely "*d*-plane pH")

$$pH_d = pH + \frac{\beta e}{\ln 10}\psi_d \tag{34}$$

the curves for different ionic strengths fall together onto a so-called mastercurve $\sigma = \sigma(pH_d)$ (bold line in Figure 2a). Such mastercurves have been discussed extensively by Riemsdijk et al.[21,22] From the equilibrium conditions given by eqs 9, 16, and 20, the derivative of eq 34 with respect to the equilibrium charge density $\sigma$ follows as

$$\frac{d(pH_d)}{d\sigma} = \frac{\beta e}{\ln(10)}\left[\frac{d\sigma^I(\psi_d)}{d\psi_d}\right]^{-1} = -\frac{\beta e}{C^I \ln(10)} \tag{35}$$

From eq 35 it is evident that the mastercurve $\sigma(pH_d)$ is in fact identical to the function $\sigma^I(\psi_d)$ (up to a factor of $\ln(10)/\beta e$ and a shift in the argument). In the case of carboxyl latex, we observe the typical S-shaped curves. For the silica surface, we can see the saturation with protonated sites at low pH, but only a small fraction of the theoretical maximum charge ($-1.3$ C/$m^2$) can actually be realized within the experimental window.

The iron hydroxide has a point of zero charge at pH = p$K$. We also notice a fairly steep and straight mastercurve. Saturation would be achieved at a very high charge densities ($\pm$493 mC/$m^2$) not accessible experimentally.

**4.3. Surface Properties upon Approach.** Since the slope of the mastercurves shows the inner layer capacity $C^I$ of the surfaces, it also reflects their regulation behavior or, more precisely, those aspects of charge regulation that are specific to the given surface material. Figure 2 illustrates this connection between the pH dependence of the isolated surface and the way surfaces interact upon approach. The charging function for the compact layer, $\sigma^I(\psi_d)$, displayed in Figure 2c for three different pH (continuous lines), is proportional the mastercurve of Figure 2a. Note that increasing the pH merely shifts the curve to the left. Its intersection with the hyperbolic sine of $\sigma^D(\psi_d,\infty)$, shown for three different ionic strengths (Figure 2c, dashed lines), gives the value $\psi_d$ and $\sigma$ in equilibrium. The derivatives of the curves in Figure 2c define the capacities $C^I$ and $C^D$ shown below (Figure 2d). The familiar diffuse layer capacity depends on the ionic strength, but is of course the same for all the materials. The $C^I$ curve on the other hand is material specific and gets shifted upon a change in pH, but does not depend on the ionic strength. Its shape and position relative to the $C^D$ curve determines the regulation behavior. Figure 2b shows the resulting regulation parameter $p$ (continuous lines) and the corresponding value for the Debye−Hückel limit (dashed lines) discussed by Carnie and Chan.[12] Whenever the diffuse layer capacitance is small compared to the inner layer capacitance, the constant potential description ($p \approx 0$) will be appropriate; in the opposite case ($C^D \gg C^D$ $p \approx 1$), the surface charge rather than the potential will stay constant as the surfaces get closer. Two surfaces which easily adjust their charge density upon changes in pH (steep titration curves) will also do so when their separation is changed.

In all of our examples, we observe that the Poisson−Boltzmann result starts to deviate from the Debye−Hückel result when the surfaces are charged up (Figure 2a and b). As a general consequence of the increase in diffuse layer capacity with potential, the system will behave in a more constant charge-like fashion than the Debye−Hückel treatment would suggest, viz., $p > p$(DH). For the iron hydroxide, we obtain rather low values of $p$ at low ionic strength and close to the point of zero charge. This finding supports the common picture that "oxide surfaces are good examples of constant potential surfaces". This statement, however, is no longer true at higher ionic strengths or further away from the point of zero charge (Figure 2b). We observe a rather strong pH dependence of the regulation parameter, which, as we infer from Figure 2b and 2d, essentially results from the nonlinear dependence of the diffuse layer capacity on $\psi_d$. In the Debye−Hückel treatment, where $C^D = \epsilon\epsilon_0\kappa$ = constant, hardly any pH dependence of $p$ would be recovered. Yet, at low pH we find that $p$ is actually closer to 1 than to 0, and so the regulation will rather resemble the limit of constant charge than the one of constant potential.

The behavior of the potential in the limit of contact can also be inferred from Figure 2c. As mentioned above, the surfaces will eventually be decharged completely when they touch each other; decreasing their distance, will decrease $\sigma^D(\psi_d,L)$. At contact, the equilibrium potential, which is given by the

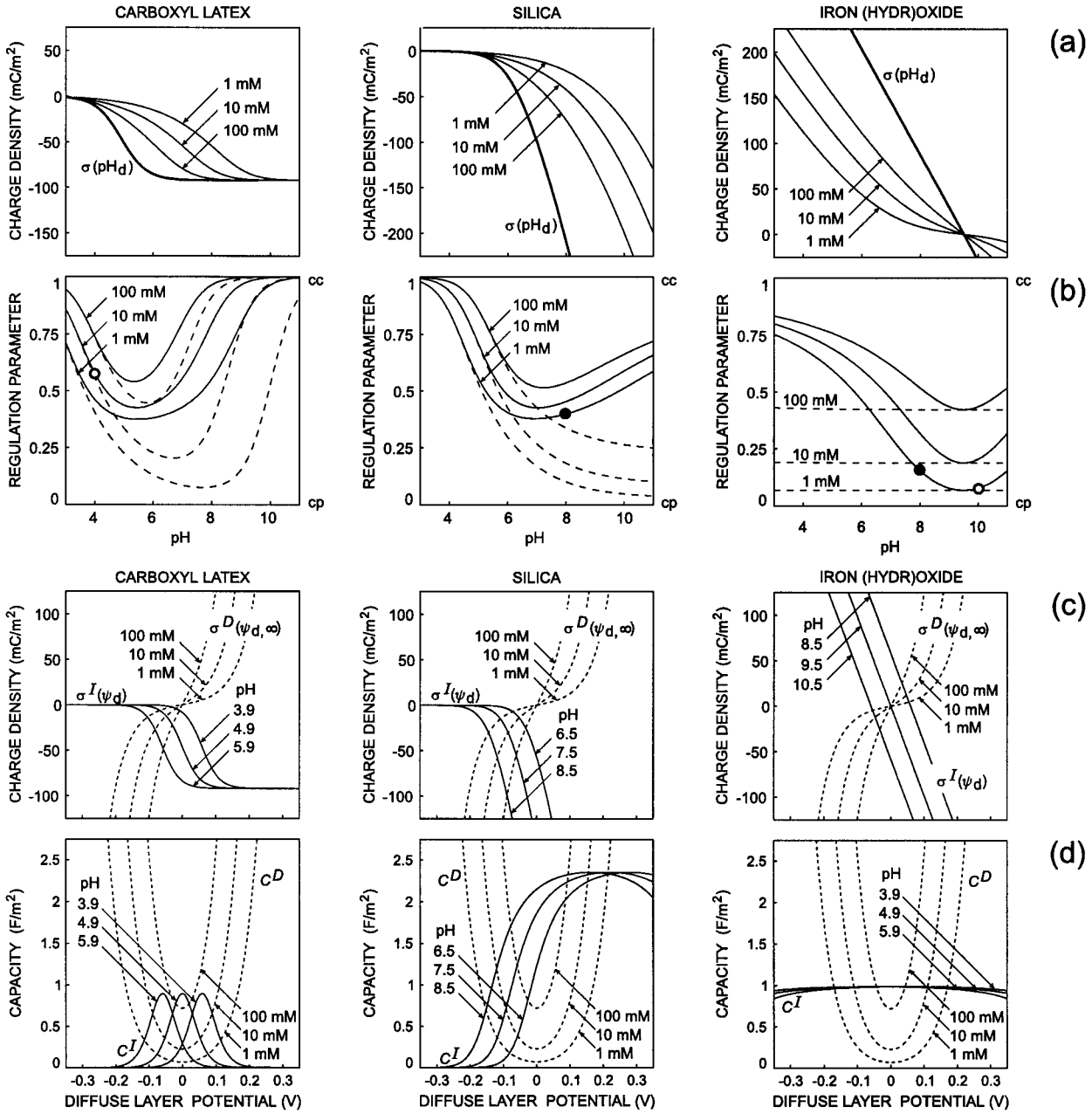


**Figure 2.** The regulation behavior as inferred from the charging of the isolated surfaces. (a) The predicted titration curves for three typical surfaces at three ionic strengths. The bold line represents the mastercurve $\sigma(\mathrm{pH_d})$. (b) The regulation parameter $p$ for the same range of pH. Continuous lines represent the results on the Poisson−Boltzmann level, the corresponding Debye−Hückel results are shown in dashed lines. The points marked by a full or open circle correspond to conditions further described in the following figures. (c) The charge−potential relation as given by the functions $\sigma^{\mathrm{I}}(\psi_{\mathrm{d}})$ and $\sigma^{\mathrm{D}}(\psi_{\mathrm{d}},\infty)$ of eqs 9 and 16. The curve $\sigma^{\mathrm{D}}(\psi_{\mathrm{d}},\infty)$ is plotted for the three ionic strengths considered before; the curve $\sigma^{\mathrm{I}}(\psi_{\mathrm{d}})$ is shown for three different values of pH. (d) The diffuse layer capacity $C^{\mathrm{D}}$ and inner layer capacity $C^{\mathrm{I}}$ given by the derivative of the curves in 2c.

intersection of $\sigma^{\mathrm{D}}(\psi_{\mathrm{d}},L)$ and $\sigma^{\mathrm{I}}(\psi_{\mathrm{d}})$, lies on the curve $\sigma^{\mathrm{I}}(\psi_{\mathrm{d}})$ as $\sigma$ tends to zero. In this limit, the curve $\sigma^{\mathrm{I}}(\psi_{\mathrm{d}})$ for the carboxyl latex and the silica surface is seen to reach zero charge only asymptotically at infinite negative potential; eq 6 implies that the potential on these types of surfaces actually diverges logarithmically upon approach. The iron hydroxide surface, however, assumes a finite electrostatic potential at contact (Figure 2c), which by eq 6 is just the Nernst potential. Whenever the isolated potential is already close to this contact value (i.e., for low ionic strength), the potential will obviously be only weakly dependent on the surface separation.

Figures 3 and 4 show how the equilibrium potential and charge density depend on the surface separation. Results are given for the silica (Figures 3a and 4a) and the iron hydroxide (Figures 3b and 4b) at an ionic strength of 1 mM and a pH of 8 (the corresponding regulation parameters $p \simeq 0.15$ for the oxide and $p \simeq 0.4$ for the silica are marked by a black dot in Figure 2b). Again, the results based on the Poisson−Boltzmann equation (full lines) are compared to their analogue in the Debye−Hückel case (broken lines). Three curves are plotted for both the Debye−Hückel and the Poisson−Boltzmann case: they correspond to constant charge, to constant potential and, always the curve between those two, to the case of charge regulation. (The constant functions are the same in the Debye−Hückel and Poisson−Boltzmann treatment, therefore only five different functions are actually displayed.)

We shall first discuss the electrostatic potential. For the silica (Figure 3a), neither the constant potential nor the constant charge curve is a good approximation to the true potential curve (reg). As mentioned before, the potential diverges at contact; the

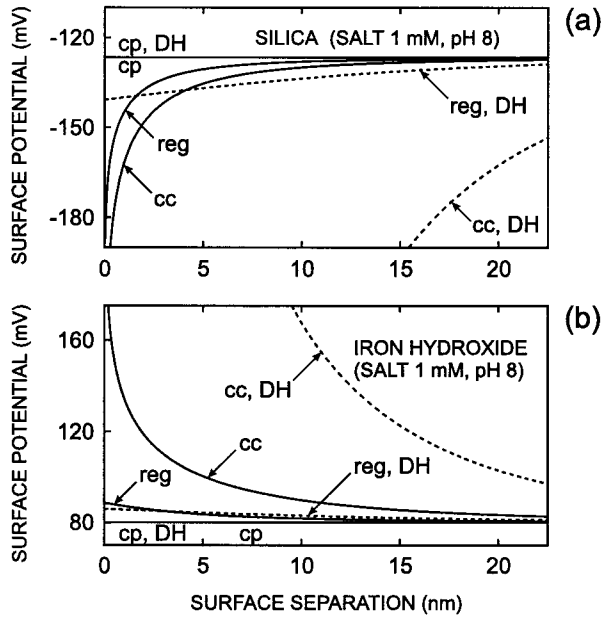


**Figure 3.** The electrostatic potential $\psi_d$ as a function of surface separation, for (a) silica and (b) iron hydroxide, both at pH 8 and an ionic strength of 1 mM (full black circles in Figure 2b). Full curves represent predictions on the Poisson−Boltzmann level, and dashed curves refer to the Debye−Hückel limit; results are given for the boundary conditions of constant charge (cc), constant potential (cp), and charge regulation (reg). In the constant potential case, the Poisson−Boltzmann curve and the Debye−Hückel curve are identical. Under charge regulation the surface potential of silica diverges upon contact, while the iron hydroxide surfaces reach the Nernst potential.

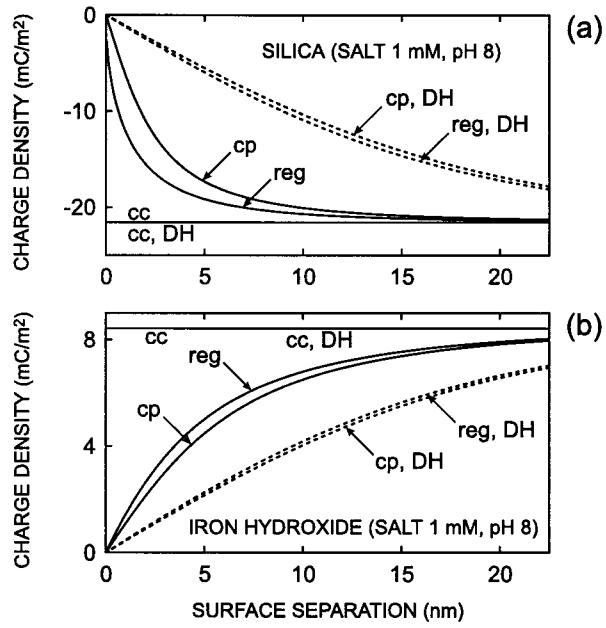


**Figure 4.** The charge density as a function of surface separation in the same representation as Figure 3. (a) Results for silica surfaces. While, according to Poisson−Boltzmann theory, the charge density under regulation conditions (reg) goes to zero at quite a different pace than the constant potential curve (cp), Debye−Hückel theory predicts the regulation to be essentially constant-potential-like. (b) For iron hydroxide surfaces, even the Poisson−Boltzmann result for charge regulation is close to the constant potential limit. The observed tendencies for both types of surfaces could also be predicted from the corresponding regulation parameter (full black circles in Figure 2b).

Debye−Hückel curve for regulation, however, goes to a finite value. The Debye−Hückel prediction for constant charge is way off the truth even at fairly large distances.

For the iron hydroxide (Figure 3b), we expectedly obtain a curve for the regulated potential (reg) that lies very close to the constant potential limit. At contact, it reaches the Nernst potential of 89 mV, which is only slightly larger than the isolated potential of 80 mV (constant potential value). The constant charge curve grossly overestimates the potential at small distances and gives a poorer approximation than the constant potential curve throughout the whole distance range; it is not quite as bad, though, as the Debye−Hückel approximation (DH) in the constant charge limit. The regulated DH curve is seen to perform quite well.

Looking at the charge densities now (Figure 4), we primarily note the major drawback in all constant charge curves of not recovering the complete decharging upon contact. Unsurprisingly, the constant potential curve lies closer to the true charge density in the case of iron hydroxide than in the case of silica. On the Debye−Hückel level, the constant potential curve and the regulated curve are almost indistinguishable, even for silica. This feature can be understood from Figure 2b for silica, where we have already seen that the Debye−Hückel treatment at high pH predicts a regulation that is unrealistically close to the constant potential limit.

**4.4. Resulting Interaction.** We shall now look at the force that interacting surfaces experience according to our model, at the interaction energy, and at the rate of aggregation we would expect from such an energy profile if the surfaces belonged to particles in a charge-stabilized colloidal suspension.

*Measurable Force.* The Derjaguin approximation to the force $F$ per radius between two surfaces in the sphere-wall or crossed-cylinder geometry are displayed in Figure 5. Again, full lines represent constant charge, constant potential, and regulation predictions on the Poisson−Boltzmann level, and broken lines show the analogues of the Debye−Hückel level. The Debye−Hückel treatment was slightly modified with respect to the previous figures: Instead of using the "bare" potential $\psi_d^\infty$ of Figures 3 and 4 in eq 30, we have used the "effective" potential $\psi_d^{eff}$, which is lower than $\psi_d^\infty$ (see Appendix). This modification is necessary to make the forces, interaction energies, etc., obtained from the Poisson−Boltzmann equation and from the Debye−Hückel equation coincide at large distances. A nonretarded van der Waals attraction

$$F_{vdW}(L)/R = \frac{A}{6L^2} \tag{36}$$

with Hamaker constants $A$ according to Table 1 has been added to the electrostatic interaction. For consistency, we use the Derjaguin approximation in the expression for the dispersion forces as well. At separations below 15 nm all Poisson−Boltzmann curves, for silica and iron hydroxide, lie between the Debye−Hückel solution for constant charge and the Debye−Hückel results for charge regulation and constant potential. The reason why the Debye−Hückel constant charge approximation generally overestimates the interaction so drastically becomes apparent in Figure 1: the Debye−Hückel constant charge treatment confounds the hatched area between the Poisson−Boltzmann curves, which is proportional to the interaction energy, with the huge area of the triangle enclosed by $\sigma_{DH}^D(\psi_d,\infty)$, $\sigma_{DH}^D(\psi_d,L)$, and $\sigma = \sigma^\infty =$ constant. Especially for the highly charged silica, the differences in the force due to different regulation behavior are of minor importance in the Poisson−Boltzmann treatment, which can also be understood as a general feature of high potential situations from Figure 1.

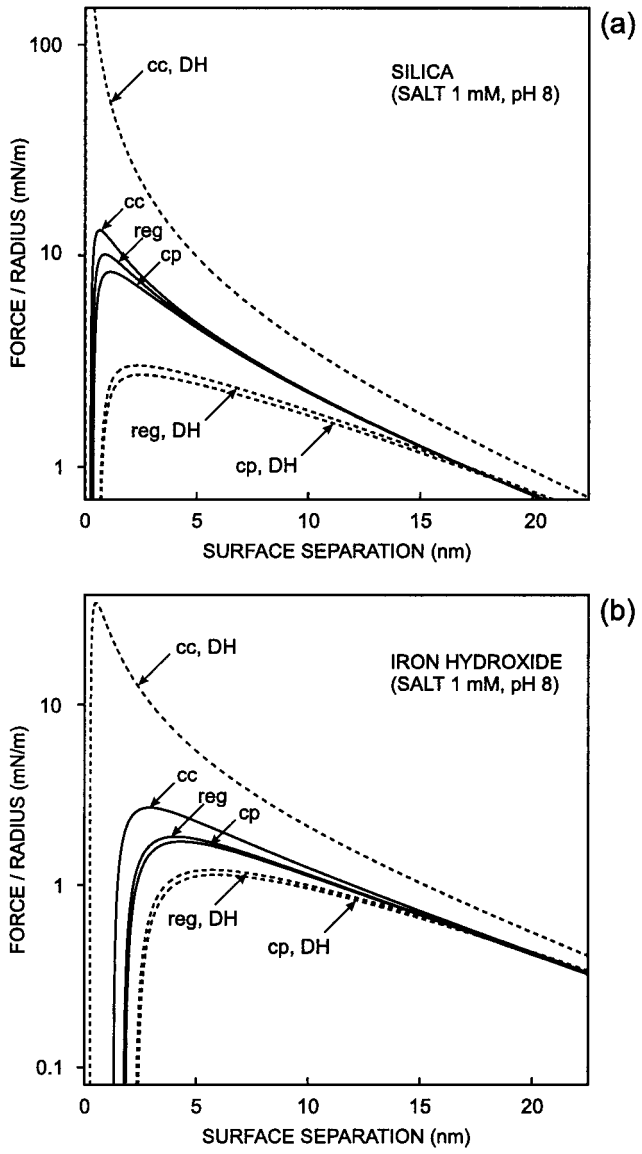


**Figure 5.** The predicted total force per radius in a sphere−wall or crossed cylinder geometry (measurable with the direct force apparatus or the atomic force microscope). Again, the Poisson−Boltzmann result (full lines) is compared to the Debye−Hückel treatment (broken lines) for the boundary conditions of constant charge, constant potential and charge regulation. Regulation parameters are the same as in Figures 3 and 4 (and correspond to the full black circles in Figure 2b). A nonretarded van der Waals contribution has been added to the purely electrostatic force, and for the Debye−Hückel curves, the bare surface charge and potential have been replaced by the corresponding *effective* values that yield the correct long distance behavior (cf. Appendix).

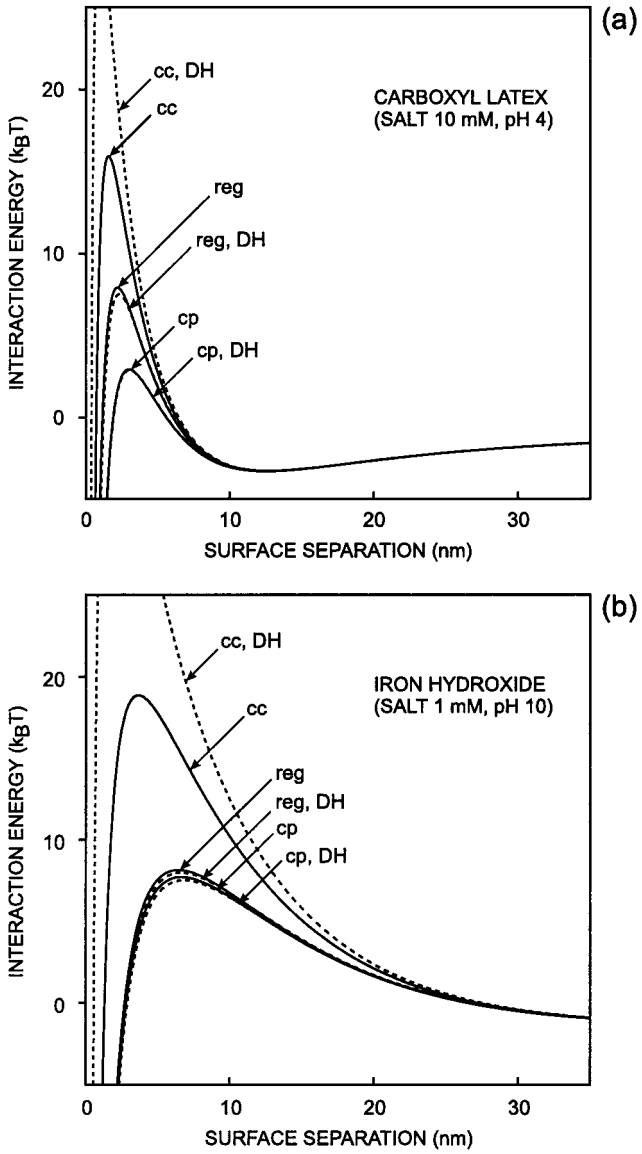


**Figure 6.** The predicted total pair interaction energy (accessible in measurements with optical tweezers or through total internal reflection microscopy). Curves are shown for (a) carboxyl latex spheres of 150 nm radii and (b) iron hydroxide spheres of 60 nm radii; regulation parameters correspond to the open circles in Figure 2b. The surface potential $\psi_d^\infty$ of the isolated surface is 21 mV for the carboxyl latex and 27.5 mV for the iron hydroxide. Differences in the general shape of the curves in a and b are mainly due to the different ionic strength.

Nonetheless we see that, in the case of silica the true, regulated force lies roughly in the middle between the constant charge and constant potential curve, while in the case of the iron hydroxide it is clearly closer to the constant potential result than to the constant charge result. The difference in the position of the force maximum for the two materials is due to their very different Hamaker constants (Table 1).

*Pair Interaction Energy.* In Figure 6, the same six types of curves (constant potential, constant charge, regulation, on the Debye−Hückel and Poisson−Boltzmann level) are shown for the pair interaction energy $V$ (including again the van der Waals attraction) of carboxyl latex spheres at pH 4 in a 10 mM solution of monovalent electrolyte and for iron hydroxide spheres at pH 10 in a 1 mM electrolyte solution. These conditions should imply an intermediate regulation behavior for the latex ($p \simeq 0.57$) and a constant-potential-like behavior for the iron hydroxide ($p \simeq 0.08$); the corresponding points in Figure 2b are marked by an open circle. (The Hamaker constants are given in Table 1.) For the latex, the regulated curve lies roughly halfway between the two limiting cases, at separations of 3−10 nm, where the differences first become important. For the iron hydroxide, all energy curves for the regulated case and the constant potential case lie very close together indeed, while the constant charge prediction is far off, especially in the Debye−Hückel treatment. In Figure 6, the predictions on the Debye−Hückel level, except for the constant charge limit, do not differ as much from the ones of the Poisson−Boltzmann approach as in Figure 5 simply because the potentials involved are not very high. The difference between Figure 6a and b with respect to the general shape and position of the energy peak is due to the differences in the Hamaker constants and in the electrolyte concentration.

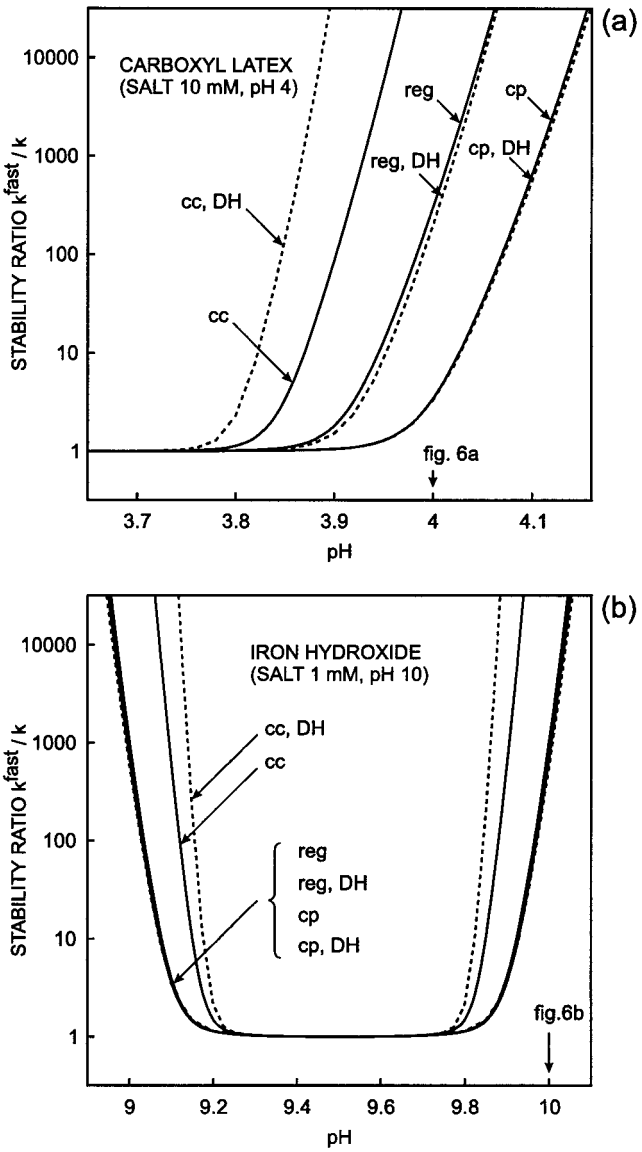


**Figure 7.** The stability ratio as a function of pH. (a) For carboxyl latex spheres (150 nm) at an ionic strength of 10 mM, the true regulation behavior is not described correctly by the constant charge or the constant potential result. (b) In the case of iron hydroxide (60 nm) at an ionic strength of 1 mM, the four curves corresponding to constant potential conditions and charge regulation in the Poisson−Boltzmann (full lines) and Debye−Hückel (broken lines) treatment almost fall together, only the two curves for constant charge conditions (inner curves) are clearly distinguished from them.

*Aggregation of Particles in Colloidal Suspensions.* The implications of the different regulation behavior of carboxyl latex in a 10 mM solution and an iron hydroxide in 1 mM solution on the stability of their colloidal suspensions are illustrated in Figure 7.

We have plotted the so-called stability ratio $k^{fast}/k$. The dimer formation rate constant $k$ is related to the interaction energy via

$$k = 4\pi\left\{\int_{2R}^{\infty} \frac{\exp[\beta V(r)]}{r^2 D(r)}\,dr\right\}^{-1} \qquad (37)$$

where $D(r)$ is the relative diffusion coefficient for two spheres of radius $R$ and center-to-center-distance $r = 2R+L$. The diffusion coefficient is governed, at small particle separations, by the effect of hydrodynamic interaction and was computed here in a form proposed by Honig and Wiersema.[36] The rate of fast aggregation $k^{fast}$ is defined by eq 37 in the absence of electrostatic repulsion.

Figure 7a shows the predicted increase of colloid stability for the carboxyl latex; the different curves correspond to the same six cases discussed in the previous figures. Charge regulation is seen to have a large effect on stability and in this case the differences between the prediction for full regulation (reg) and both limiting conditions (cc and cp) are very clear. In recent experiments on carboxyl latex particles, such DLVO predictions of colloidal stability were seen to work quantitatively at ionic strengths up to 10 mM.[29]

The stability of iron hydroxide on both sides of the point of zero charge is shown in Figure 7b. The two inner curves are the Debye−Hückel and Poisson−Boltzmann prediction in the constant charge limit, the other four curves almost fall together, so small is here the influence of nonlinearity and so little does the full charge regulation differ from the constant potential behavior in terms of aggregation rates in this system.

*Use of the Regulation Parameter at Small Distances.* The predictions of separation dependent properties (Figures 3−7) indicate that our regulation parameter $p$ (eq 27) does indeed reflect the regulation behavior correctly even at separations of several nanometers, although this parameter is expressed entirely through properties of the isolated surface.

Knowing the regulation parameter is particularly useful when only the solutions for constant charge and constant potential interaction are available from calculations (which is a rather common situation). Charge regulation can then easily be accounted for by approximating, e.g., the true interaction energy per unit area by the combination

$$W_{approx}(L) = W^{(cp)}(L) + p[W^{(cc)}(L) - W^{(cp)}(L)] \qquad (38)$$

The quality of such an approximation is shown in Figure 8, where we have plotted the relative error

$$\text{error}(L) = \frac{W_{approx}(L) - W^{(reg)}(L)}{W^{(reg)}(L)} \times 100\%$$

for the exemplary cases discussed earlier and compared it to the corresponding error in the pure constant charge and constant potential assumption (all curves calculated on the Poisson−Boltzmann level). Only at very small separations do we see considerable deviations of the approximation from the true result from the nonlinear boundary condition of charge regulation (reg), which corresponds to the zero line in Figure 8. At a separation of one Debye length, the error is less than 5% in all the cases considered and considerably lower than the error of both the constant charge and constant potential assumption. This observation is particularly remarkable in the case of the iron hydroxide: while we have seen before that this material is generally well described by the constant potential assumption, our approximation $W_{approx}$ shows a spurious divergence at contact, caused by the constant charge contribution in eq 38. Still the approximation 38 based on the interaction parameter $p$ is more accurate than the constant potential result down to separations of much less than a Debye length.

## 5. Conclusions

The origin and the effects of charge regulation for surfaces of different charging characteristics can be described within the 1-p$K$−basic Stern model. A criterion of whether surfaces interact at constant charge or constant potential has been formulated

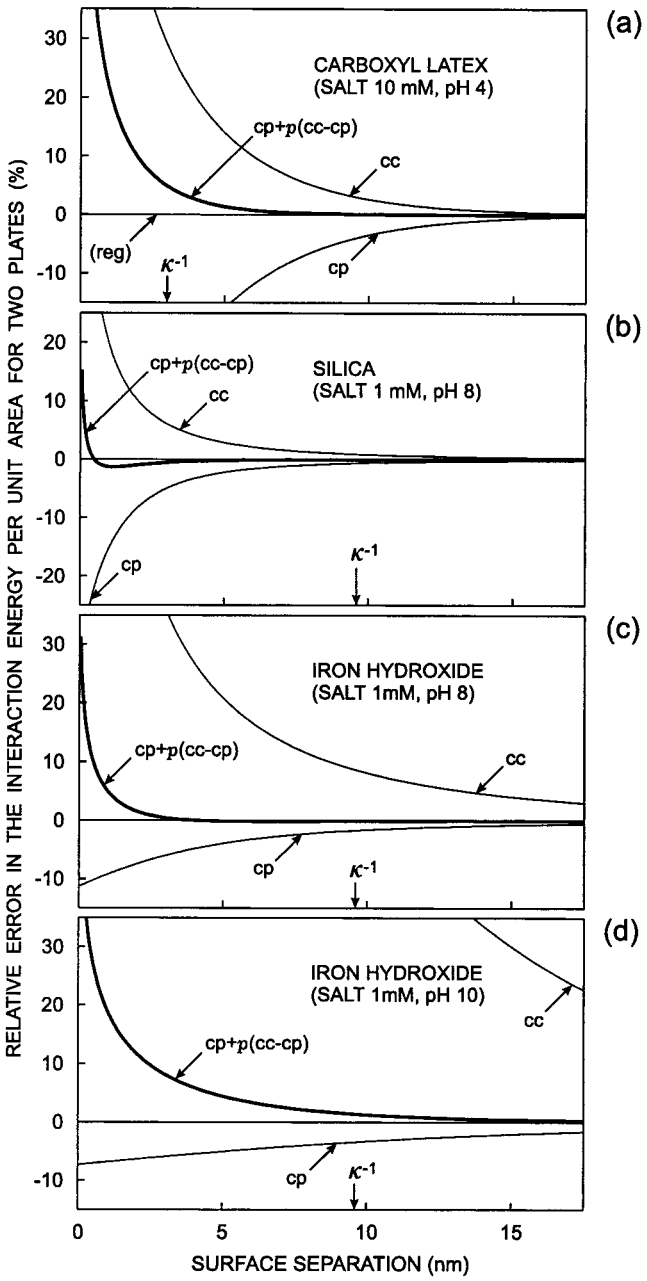


**Figure 8.** The relative error made by approximating the interaction energy $W^{(reg)}$ by the constant charge expression $W^{(cc)}$, by the constant potential expression $W^{(cp)}$, or by the approximation $pW^{(cc)} + (1 - p)W^{(cp)}$, using the regulation parameter $p = C^D/(C^D + C^I)$ corresponding to the filled and open circles in Figure 2b.

for arbitrary potentials in terms of a single regulation parameter. This parameter relates the true interaction energy to the energy in the two limiting cases where it takes the values 0 and 1. A graphical interpretation shows that the intermediate behavior typically encountered in real systems depends on the interplay of the capacities associated with the diffuse part and the inner (compact) part of the electric double layer: if the diffuse layer capacity dominates, the constant charge model will be a good approximation; if the inner layer capacity dominates, the constant potential assumption is appropriate. This statement was verified quantitatively for surface separations of several nanometers. For the isolated surface, the value of the inner layer capacity can be inferred from acid−base titration curves; the diffuse layer capacity is given by the Grahame equation. The charge regulation for interacting surfaces is connected to their ability of adjusting charge densities to changes in pH, because the variation of charge with surface separation is triggered by changes in the local proton concentration near the surfaces. Approximations were judged by comparison with the solution of the Poisson−Boltzmann equation for full charge regulation. We have shown that a local linearization of the charge−potential relation for both the diffuse and the compact inner layer around the long distance limit gives a more accurate picture at high potentials than the global linearization carried out in Debye−Hückel approximation. The regulation behavior has been discussed in detail for the exemplary cases of carboxyl latex, silica, and iron hydroxide surfaces. Upon contact, all surfaces get fully decharged; at the same time, the electrostatic potential of carboxyl latex and silica diverges, whereas the potential of amphoteric surface reaches the Nernst value. The effect of charge regulation on the interaction force and energy, as well as on the aggregation kinetics was shown to be in good agreement with our regulation criterion.

**Acknowledgment.** We thank Subir Bhattacharjee and Hans Sticher for different types of support. This work was financed by the Swiss National Science Foundation.

## Appendix

For the dimensionless potential $\Phi = \beta e\psi(x)$ the Poisson−Boltzmann equation reads

$$\frac{d^2\Phi}{dx^2} = \kappa^2 \sinh \Phi \tag{A.1}$$

The first integration can be carried out explicitly after multiplication with $d\Phi/dx$ using the boundary condition $d\Phi/dx = 0$ for $x = 0$:

$$\left(\frac{d\Phi}{dx}\right)^2 = 2\kappa^2 (\cosh \Phi - \cosh \Phi_m) \tag{A.2a}$$

with $\Phi_m = \Phi(0)$. Introducing the abbreviations $\Omega(x) = \exp[\Phi(x) - \Phi_m]$ and $\xi = \exp(\Phi_m)$, we obtain

$$\left(\Omega^{-1}\frac{d\Omega}{dx}\right)^2 = \kappa^2[(\xi\Omega)^{-1} + \xi\Omega - \xi^{-1} - \xi] \tag{A.2b}$$

Let the surfaces be negatively charged (otherwise just change the sign in the solution), then $d\Phi/dx \le 0$ for $x \ge 0$ and separation of variables yields

$$\frac{d\Omega}{\sqrt{\Omega(1-\Omega)(1-\xi^2\Omega)}} = -\frac{\kappa}{\sqrt{\xi}}\,dx \tag{A.3}$$

Upon substitution of $\Omega = \sin^2 \theta$ we have

$$-\frac{\kappa x}{2\sqrt{\xi}} = \int_{\pi/2}^{\arcsin\sqrt{\Omega}} \frac{d\theta}{\sqrt{1 - \xi^2 \sin^2 \theta}} \tag{A.4}$$

The expression

$$u = \int_0^{\varphi} \frac{d\theta}{\sqrt{1 - m \sin^2 \theta}} = F(\varphi|m)$$

defines an elliptic integral of the first kind. The special case of $F(\pi/2;m) = K(m)$ is called the corresponding *complete* integral or the quarter period of the Jacobian elliptic functions. These

functions are given by inversion of the integral $F(\varphi|m)$, they are defined as[24]

$$\mathrm{sn}(u|m) = \sin\varphi$$

$$\mathrm{cn}(u|m) = \cos\varphi = \sqrt{1 - \mathrm{sn}^2(u|m)}$$

$$\mathrm{dn}(u|m) = \sqrt{1 - m\,\mathrm{cn}^2(u|m)}$$

$$\mathrm{cd}(u|m) = \mathrm{cn}(u|m)/\mathrm{dn}(u|m)$$

where $u$ is called the argument and $m$ the parameter of the elliptic function. We will also make use of their periodicity property

$$\mathrm{cd}(u|m) = \mathrm{sn}(K(m) - u|m)$$

By splitting the integral in eq A.4

$$\int_{\pi/2}^{\arcsin\sqrt{\Omega}} f(\theta)\,\mathrm{d}\theta = \int_{0}^{\arcsin\sqrt{\Omega}} f(\theta)\,\mathrm{d}\theta - \int_{0}^{\pi/2} f(\theta)\,\mathrm{d}\theta$$

we obtain

$$-\frac{\kappa x}{2\sqrt{\xi}} = -u = \mathrm{sn}^{-1}\sqrt{\Omega} - K(\xi^2)$$

where $\mathrm{sn}^{-1}$ denotes the inverse function of $\mathrm{sn}(u|m)$ or

$$\Omega(x) = \mathrm{sn}^2(K(\xi^2) - u|\xi^2) = \mathrm{cd}^2(u|\xi^2) \qquad \text{(A.5)}$$

which is the result cited in eqs 19 and 17. With the derivative

$$\frac{\mathrm{d}}{\mathrm{d}u}\mathrm{cd}(u|m) = (m-1)\frac{\mathrm{sn}(u|\xi^2)}{\mathrm{dn}^2(u|\xi^2)}$$

we find eq 18 for the charge density

$$\sigma = \frac{\epsilon\epsilon_0}{\beta e}\frac{\mathrm{d}\Phi}{\mathrm{d}x} = \frac{\epsilon\epsilon_0\kappa}{\beta e}\frac{\xi^2 - 1}{\sqrt{\xi}}\frac{\mathrm{sn}(u|\xi^2)}{\mathrm{cn}(u|\xi^2)\,\mathrm{dn}(u|\xi^2)}$$

Since we have $\mathrm{cn}(0|m) = \mathrm{dn}(0|m) = 1$ and $\mathrm{sn}(0|m) = u$, it follows that

$$\sigma \to 0 \qquad \text{as} \qquad L \to 0$$

irrespective of the material properties of the surface. Equating $\sigma^{\mathrm{I}}(\psi_{\mathrm{d}})$ and $\sigma^{\mathrm{D}}(\psi_{\mathrm{d}},L)$, namely by inserting eqs 18 and 19 into eq 9, leaves us with a single transcendental equation for $\xi$. Once it is solved, the interaction force and energy for the plates follow directly from equations 23−25.

For large surface separations ($\kappa L > 20$), we have used the linearized expression 30 instead. One then has to replace the electrostatic potential $\psi_{\mathrm{d}}^{\infty}$ of the isolated surface by the "effective" potential[2]

$$\psi_{\mathrm{eff}} = \frac{4}{\beta e}\tanh\left(\frac{\beta e}{4}\psi_{\mathrm{d}}^{\infty}\right) \qquad \text{(A.6)}$$

which in the linear theory yields the same potential decay for long distances $x$ form the isolated surface, as the true, bare potential does in the nonlinear treatment.[2] Because of the hyperbolic tangent in equation (A.6), the corresponding effective charge density $\sigma_{\mathrm{eff}} = \epsilon\epsilon_0\kappa\psi_{\mathrm{eff}}$, related to $\psi_{\mathrm{eff}}$ by the linearized version of eq 16, saturates for high bare charge into a maximum value also known as the condensation limit.[37,38]

## References and Notes


(1) Israelachvili, J. *Intermolecular & Surface Forces*, 2nd ed.; Academic Press: London, 1992.

(2) Russel, W. B.; Saville, D. A.; Schowalter, W. R. *Colloidal Dispersions*; Cambridge University Press: Cambridge, 1989.

(3) Ninham, B. W.; Yaminsky, V. *Langmuir* **1997**, *13*, 2097.

(4) Derjaguin, B. V.; Landau, L. *Acta Physicochim. USSR* **1941**, *14*, 633.

(5) Verwey, E. J. W.; Overbeek, J. Th. G. *Theory of the Stability of Lyophobic Colloids*; Elsevier: Amsterdam, 1948.

(6) Ninham, B. W.; Parsegian, V. A. *J. Theor. Biol.* **1971**, *31*, 405.

(7) Chan, D. Y. C.; Perram, J. W.; White, L. R.; Healy, T. W. *J. Chem. Soc., Faraday Trans. 1* **1976**, *71*, 1046.

(8) Healy, T. W.; White, L. R. *Adv. Colloid Interface Sci.* **1978**, *9*, 303.

(9) Chan, D. Y. C.; Mitchell, D. J. *J. Colloid Interface Sci.* **1983**, *95*, 193.

(10) Chan, D. Y. C. Geochemical Processes at Mineral Surfaces; (Davis, J. A., Hayes, K. F., Eds.; ACS Symposium Series 323; American Chemical Society, Washington, DC, 1986; p 99.

(11) Krozel, J. W.; Saville, D. A. *J. Colloid Interface Sci.* **1992**, *150*, 365.

(12) Carnie, S. L.; Chan, D. Y. C. *J. Colloid Interface Sci.* **1993**, *161*, 260.

(13) Carnie, S. L.; Chan, D. Y. C. *J. Colloid Interface Sci.* **1993**, *155*, 297.

(14) Reiner, E. S.; Radke, C. J. *Adv. Colloid Interface Sci.* **1993**, *47*, 59.

(15) Hsu, J.-P.; Tseng, M.-T. *J. Colloid Interface Sci.* **1996**, *182*, 609.

(16) Pujar, N. S.; Zydney, A. L. *J. Colloid Interface Sci.* **1997**, *192*, 338.

(17) Behrens, S. H.; Borkovec, M. *J. Chem. Phys.* In press.

(18) Harding, I. H.; Healy, T. W. *J. Colloid Interface Sci.* **1985**, *107*, 382.

(19) Westall, J.; Hohl, H. *Adv. Colloid Interface Sci.* **1980**, *12*, 265.

(20) Gouy, G. *J. Phys. Radium* **1910**, *9*, 457. Chapman, D. L. *Philos. Mag.* **1913**, *25*, 475;

(21) De Wit, J. C. M.; Van Riemsdijk, W. H.; Nederlof, M. M.; Kinniburgh, D. G.; Koopal, L. K. *Anal. Chim. Acta* **1990**, *232*, 189.

(22) De Wit, J. C. M.; Van Riemsdijk, W. H.; Koopal, L. K. *Environ. Sci. Technol.* **1990**, *27*, 2005.

(23) Hunter, R. J. *Foundations of Colloid Science*; Oxford University Press: Oxford, 1989.

(24) Abramowitz, M.; Stegun, A. *Handbook of Mathematical Functions*; 9th ed.; Dover Publications: New York, 1972.

(25) Israelachvili, J. N.; Adams, G. E. *J. Chem. Soc., Faraday Trans.* **1978**, *74*, 975. Pashley, R. M. *J. Colloid Interface Sci.* **1980**, *80*, 153. Israelachvili, J. N. *Adv. Colloid Interface Sci.* **1982**, *16*, 31.

(26) Hartley, P. G.; Larson, I.; Scales, P. J. *Langmuir* **1997**, *13*, 2207.

(27) Crocker, D.; Grier, D. *Phys. Rev. Lett.* **1994**, *73*, 352. Crocker, D.; Grier, D. *Phys. Rev. Lett.* **1996**, *77*, 1897. Sugimoto, T.; Takahashi, T.; Itoh, H.; Sato, S. I.; Muramatsu, A. *Langmuir* **1997**, *13*, 5528.

(28) Prieve, D. C.; Bike, S. G.; Frey, N. A. *Faraday Discuss. Chem. Soc.* **1990**, *90*, 209. Frey, N. A.; Prieve, D. C. *J. Chem. Phys.* **1993**, *98*, 7552. Liebert, R. B.; Prieve, D. C. *Biophys. J.* **1995**, *69*, 66.

(29) Behrens, S. H.; Borkovec, M.; Schurtenberger, P. *Langmuir* **1998**, *14*, 1951.

(30) Behrens, S. H.; Christl, D. I.; Emmerzael, R.; Schurtenberger, P.; Borkovec, M. To be published.

(31) Hiemstra, T.; van Riemsdijk, W. H.; Bolt, G. H *J. Colloid Interface Sci.* **1989**, *133*, 91. Hiemstra, T.; de Wit, J. M. C.; van Riemsdijk, W. H. *J. Colloid Interface Sci.* **1989**, *133*, 105.

(32) van Riemsdijk, W. H. Internal report. Wageningen Agricultural University: The Netherlands, 1979. Bolt, G. H.; van Riemsdijk, W. H. In Soil Chemistry. B. Physio-chemical Models, 2nd ed.; Bolt, G. H., Ed.; Elsevier: Amsterdam, 1982; p 459. Chan, D. Y. C. *Geochemical Processes at Mineral Surfaces*; Davis, J. A., Hayes, K. F., Eds.; ACS Symposium Series 323; American Chemical Society: Washington, DC, 1986; p 99.

(33) Hiemstra, T.; van Riemsdijk, W. H. *J. Colloid Interface Sci.* **1996**, *179*, 488.

(34) Borkovec, M. *Langmuir* **1997**, *13*, 2608.

(35) Schudel, M.; Behrens, S. H.; Holthoff, H.; Kretzschmar, R.; Borkovec, M. *J. Colloid Interface Sci.* **1997**, *196*, 241.

(36) Honig, E. P.; Roebersen, G. J.; Wiersema, P. H. *J. Colloid Interface Sci.* **1971**, *36*, 97.

(37) Alexander, S.; Chaikin, P. M.; Grant, P.; Morales, G. J.; Pincus, P.; Hone, D.; *J. Chem. Phys.* **1984**, *80*, 5776.

(38) Gisler, T.; Schulz, S. F.; Borkovec, M.; Sticher, H.; Schurtenberger, P.; D'Aguanno, B.; Klein, R. *J. Chem. Phys.* **1994**, *101*, 9924.